Scientific Research Publishing

Open Journal of Fluid Dynamics, 2025, 15(3), 158-174
https://www.scirp.org/journal/ojfd
ISSN Online: 2165-3860
ISSN Print: 2165-3852

Experimental Study of the Motion Response of a Bionic Manta Ray Vehicle Model under Regular Wave

Hanhai Lin, Jiemin Zhan, Wei Su*, Ziwei Huang, Wenqing Hu

Department of Applied Mechanics and Engineering, Shenzhen Campus of Sun Yat-sen University, Shenzhen, China
Email: *suwei@mail.sysu.edu.cn

How to cite this paper: Lin, H.H., Zhan, J.M., Su, W., Huang, Z.W. and Hu, W.Q. (2025) Experimental Study of the Motion Response of a Bionic Manta Ray Vehicle Model under Regular Wave. *Open Journal of Fluid Dynamics*, **15**, 158-174.
https://doi.org/10.4236/ojfd.2025.153010

Received: June 22, 2025
Accepted: August 1, 2025
Published: August 4, 2025

Abstract

The wave buoy analogy is mostly applied to ships, while its application in manta ray bionic vehicles is less frequently addressed. However, the vehicle needs to obtain wave direction information to adjust its own attitude when operating on the ocean surface. This study discusses a method for obtaining current main wave direction information for a manta ray bionic vehicle. Systematic wave tank experiments were performed to examine the relationship between the pitch, roll, and wave incidence direction of the vehicle. One of the important results is that the phase difference in the roll and pitch motion of the manta ray vehicle model at 30 and 60 degrees headings is very similar, while at 120 and 150 degrees, they are in anti-phase. Another result is that the directional parameter curve calculated from the power spectrum of the rolling and pitching motion time series data is symmetrical about a 90-degree wave direction. The conclusion of this study is that the manta ray bionic vehicle has excellent wave-following performance and can obtain information about the current main wave direction through the relationship between its roll and pitch movements and the relative incident wave direction.

Keywords

Wave Tank Experiments, Manta Ray Bionics, Floating Bodies, Wave Direction, Wave Buoy Analogy

1. Introduction

With the growing demand for marine scientific research and monitoring of the marine environment in remote areas of the ocean, oceanographic vehicles, as important equipment for ocean exploration, have attracted the attention of research-

ers in various countries. According to the different working methods and functions, they can be divided into Remote Operated Vehicle (ROV) and Autonomous Underwater Vehicle (AUV), which are usually connected to the mother ship or base station by cables to transmit energy and data. The AUV supplies energy to each module through its own power supply, and at the same time uses its own sensors to collect the information it needs to make the next decision with the information it collects. When the AUV rises to the surface for autonomous operation, it needs to collect the current wave information to make the next behavioral decision, in which the collection of the current wave direction information allows the navigator to adjust its cross-wave, wave-facing, or wave-following attitude [1], so as to meet the needs of the task of utilizing wave energy to replenish energy [2]. The underwater biometric flapping wing navigators modeled on manta rays have a broad application prospect. The propulsion mode of manta rays is central or paired-fin propulsion, which is realized by pairs of pectoral fins flapping to generate thrust. Based on this propulsion mode and the overall structure of manta rays, the design of manta ray bionic underwater flap navigator can be combined with solar power generation technology or wave energy conversion technology [3], which enables the navigator to float on the surface of the sea to utilize solar energy or ocean energy to realize self-supply of energy in standby mode or when the supply of battery power is insufficient, so that the endurance of the navigator can be prolonged without the need to carry additional equipment.

Currently the main ways commonly used to obtain wave direction information are: remote sensing measurement, fixed-point measurement, and body-following measurement. Remote swing measurement is to use satellite or shipboard radar equipment to obtain image information of a wide range of sea areas, and then through the processing of the sea surface image to obtain the wave spectrum; fixed-point measurement is to use wave buoys or wave meter arrays and other equipment to collect wave information; the accompanying body measurement is a method to analogize the ships and other navigational vehicles into wave buoys [4], through the collection of the navigational vehicles in the wave excitation of the oscillating motion response Dirdal proposed a phase-time-path-differences method, which utilizes the phase-time-path differences of the motion response of a sensor array on a ship under wave action to determine the direction and wave number of waves in real time, was validated on ship models and solid ships [5] [6]. Selimović proposes an attention-based neural network method (AT-NN) to estimate significant wave height, zero-crossing period, and relative wave direction from raw 3-DOFs ship motion time-series (pitch, roll, heave) [7]. Due to the limitation of equipment loading capacity AUV have some difficulties in obtaining wave direction information through satellite remote sensing and microwave radar, while combining the characteristics of AUV such as large autonomous activity range, high flexibility and strong self-governance ability, follower measurements based on the principle of navigator analogous to wave buoys have become a suitable method for AUV to collect information on wave direction.

Aiming at the problem of the manta ray bionic configuration AUV using its own motion response signal to recognize the main wave direction, a multi-module manta ray bionic structure flapping-wing vehicle model is fabricated, and the motion response signal generated by the vehicle under wave excitation is investigated, and the multi-module vehicle prototype model with manta ray bionic configuration is used as an experimental object to conduct the wave tank experiments. The multi-modular vehicle is divided into three modules with two pectoral fins and a central torso, and an attitude sensor is arranged in each module to collect the motion response signals of each floating body under wave excitation in several different wave directions. Using the motion response signals of roll and pitch motion of the torso module, a main wave direction estimation method based on the principle of wave direction estimation by two-axis tachometer is applied to obtain the relationship curves between the wave directions of different period incident waves and the roll and pitch motion responses of the model.

2. Model Design and Wave Direction Estimation Principle

2.1. Manta Bionic Model Design

The study primarily referenced the manta ray biological model obtained by Zhan and Cai using non-uniform rational spline three-dimensional reconstruction [8]. Some basic simplifications and modifications were made to the model during the reconstruction process. For example, in order to obtain a better streamlined biomimetic model, the manta ray's head fins and tail structure were removed. The maximum spreading length of manta rays is defined as L, of which the maximum spreading length of unilateral pectoral fins is 0.35 L, and that of the trunk is 0.3 L. Without considering the manta ray's trailing tail, the body length is about 0.5 times the spreading length, and Figure 1 shows the proportional characteristics of manta rays' bio-morphological shape.

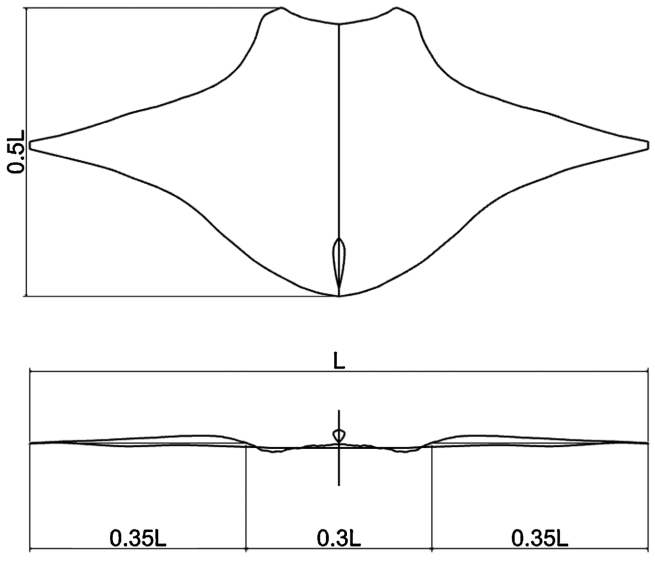

Figure 1. Illustration of manta ray model scale.

Firstly, a suitable NACA parametric airfoil was selected as the model of the navigator based on the longitudinal segment at the maximum thickness of the central torso. This longitudinal segment was used as the main configuration of the central torso and the supporting fins of the pectoral fins on both sides. The design of the navigator configuration is based on the characteristics of the manta ray's biological structure and shape. Based on the longitudinal cross-segment of the manta ray reconstruction model at the maximum thickness of the central torso portion and the internal deployment of sensor volume requirements, the NACA0020 airfoil was selected as the skeleton shape of the central torso of the navigator model. The same airfoil profile was used for the left and right flaps.

A 2-DOFs connection structure was used to connect the two sides of the pectoral fin modules, and the central torso module and the two sides of the pectoral fin modules were modeled separately. After the model skeleton was created, a photosensitive resin material with a density of 1.24 g/cm^3 was used to produce a solid model frame using 3D printing technology. Once the solid model was obtained, a waterproof nylon fabric was used as the skin material to cover the pectoral fin skeleton.

The physical model is shown in Figure 2. The structural parameters of the model are: the maximum spread length is about 320 mm, the maximum chord length is about 150 mm; the maximum spread length of the unilateral pectoral fin module is about 100 mm, the maximum spread length of the central torso module is 90 mm, the spacing between the central torso module and the left and right pectoral fin modules is 19.6 mm, and the maximum thickness is 24.9 mm. The weights of the two lateral pectoral fin modules are 46 g each, and that of the central torso module is 110 g. The draft in still water is 19.5 mm.

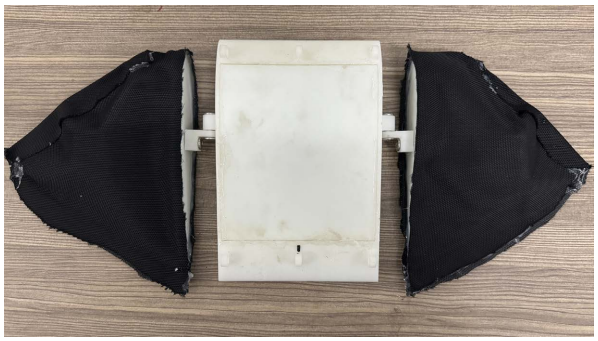

Figure 2. Manta ray bionic vehicle solid model.

2.2. Motion of a Vehicle Model in Regular Waves

First, as shown in Figure 3, the navigator as a whole is symmetrical along the left-right axis of the central torso module, however, the navigator model as a whole is not symmetrical in the *y-o-z* plane. Also, for the unilateral pectoral fin of the navigator, it is not a symmetric structure, and each module of the navigator will have different behaviors depending on the direction of the incident wave. Therefore, by investigating the relationship between the roll and pitch motions in different

wave directions, it can be found that there is a certain correlation between the model motion and the direction of the incident wave.

When the relative incident wave direction is β, the front-view, top-view and side view motion schematic of the central torso module of the relative manta ray vehicle model are shown in Figure 4(a)-(c). It can be seen that the wave passing through the multi-modular vehicle model will cause it to generate roll and pitch motion, while the multi-modular vehicle model will only generate vertical oscillatory motion when the wavelength of the incident wave is much larger than the characteristic length of the manta ray along the direction of the incident wave.

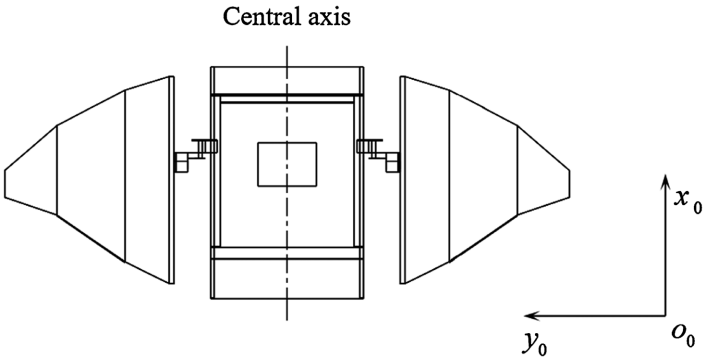

Figure 3. Central axis from top view of Manta bionic model.

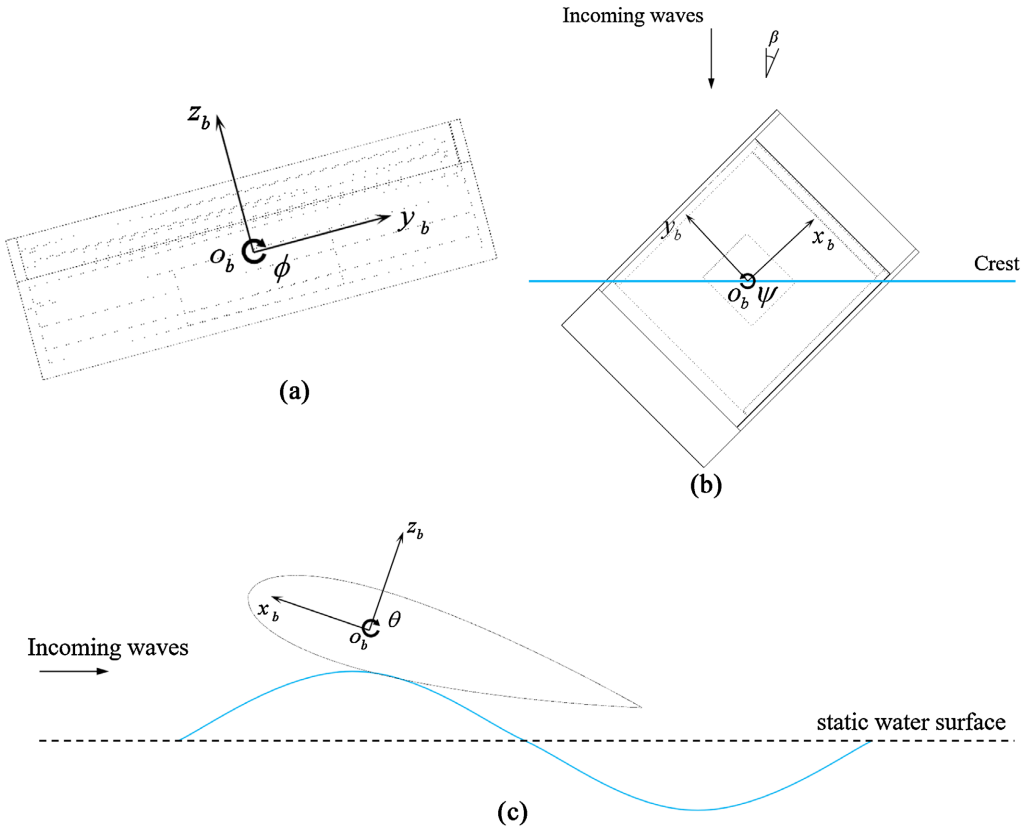

Figure 4. The motion of the body module of a manta ray bionic vehicle model under the action of regular waves from (a) Front view; (b) Top view; (c) Side view.

Therefore, the subsequent design experiments mainly consider the short-wave case.

For floating bodies in regular waves, it can be considered that the roll and pitch response can generally be express as

$$\begin{aligned} \varphi(t) &= A_{\varphi} \sin\left(\omega_e t + \varepsilon_{\varphi}\right) \\ \theta(t) &= A_{\theta} \cos\left(\omega_e t + \varepsilon_{\theta}\right) \end{aligned} \tag{1}$$

where A_{φ} and A_{θ} denote the roll and pitch amplitudes, ω_e is the wave frequency, ε_{φ} and ε_{θ} represent the phase shifts.

2.3. Principle of Estimating Main Wave Direction from Floating Body Motion

For a floating body such as a ship or a marine craft operating on the surface of the water, the motion response under wave excitation is decomposed in the *x*, *y*, and *z* axes, and there are a total of 6 DOFs (surge, sway, heave, roll, pitch, yaw). Meanwhile, due to the asymmetry of the navigator structure in the *y*-*o*-*z* plane, the output relationship between the motion response of the navigator under regular wave excitation for roll and pitch motion is not symmetrical.

The roll and pitch motion response signals of the floating body on the sea surface are appropriately transformed in the frequency domain, so that the floating body has an approximate symmetric response axis under wave excitation, which is better adapted to the change of the main wave direction. For the roll and pitch motion time-series data $\left\{\varphi(n) \mid n = 1, 2, \cdots, N\right\}$, $\left\{\theta(n) \mid n = 1, 2, \cdots, N\right\}$ of the floating body, there are corresponding power spectra $X_{\varphi}(\omega)$, $X_{\theta}(\omega)$.

In order to make the floating body have an approximate symmetric response axis under wave excitation and have better adaptability to the change of the main wave direction, roll and pitch motion of the floating body on the surface of the sea are appropriately transformed in the frequency domain [9].

$$m_{\varphi} = \int_0^{+\infty} X_{\varphi}(\omega)\mathrm{d}\omega, \quad m_{\theta} = \int_0^{+\infty} X_{\theta}(\omega)\mathrm{d}\omega \tag{2}$$

$$\begin{aligned} &P_{\theta} = \omega_{0\theta} * X\left(\omega_{0\theta}\right) / m_{\theta}, \quad Cr_0 = \pi * \exp\left(\omega_{0\varphi}\right) \\ &C_t = \sqrt{B_{\theta} / \omega_{0\theta}} + \cos\left(\omega_{0\varphi} - \omega_{0\theta}\right) / P_{\theta} \\ &Cr = Cr_0 * \left(1 + C_t\right) \\ &Y_1 = m_{\varphi}, \; Y_2 = Cr * m_{\theta} \end{aligned} \tag{3}$$

where B_{θ} is the spectral width parameter of the pitch response spectrum, and $\omega_{0\varphi}$ and $\omega_{0\theta}$ are the peak frequencies of the roll and pitch spectra, respectively. Cr_0 is the variable that equivalently transforms the roll and pitch responses into the output of a two-axis flow meter, and C_t is the focusing parameter.

Y_1 and Y_2 reflect the ratio of the main energy of the roll and pitch frequency responses of the floating body. By approximating the roll and pitch responses of the floating body in the frequency domain and converting them into symmetrical Y_1 and Y_2 outputs, a parameter curve for determining wave direction is introduced as the basis for determining the current main wave direction of the vessel.

The definitions of each parameter are as follows:

$$\begin{aligned} Para1 &= X_{\varphi}\left(\omega_{0\varphi}\right)\Big/X_{\theta}\left(\omega_{0\theta}\right), & K_1 &= Para1\Big/\max\left(Para1\right) \\ Para2 &= \tan^{-1}\left(Y_1/Y_2\right), & K_2 &= Para2\Big/\max\left(Para2\right) \end{aligned} \tag{4}$$

3. Experimental Arrangement

3.1. Experimental Environment

The experiments were carried out in the SYSU wave tank laboratory, which contains a wave basin with a length of 30 m, a width of 0.6 m, and a height of 1 m equipped with a wave maker. The water depth for all the experiments is 0.48 m. The wave maker adopts a 4-axes, 3-plates and push-sway combination wave generation method to ensure that the incident wave period and wave height are consistent for each group of experimental conditions. The total wave generation time for each group of experiments is 60 seconds, and the stable segment of wave generation is taken for analysis when analyzing the data later. A wave probe is used to record the free surface elevation. A wave absorption plate is installed at the end of the wave tank to reduce the influence of reflected waves. A wave probe is placed 5 m away from the wave maker to measure the actual incident wave height, and the experimental model is placed about 5.5 m away from the wave generator. Figure 5 shows the layout diagram of the wave tank wave generation experimental environment. Figure 6 presents the experimental configuration with the multi-plates wave generator, vessel model, and wave probe instrumentation.

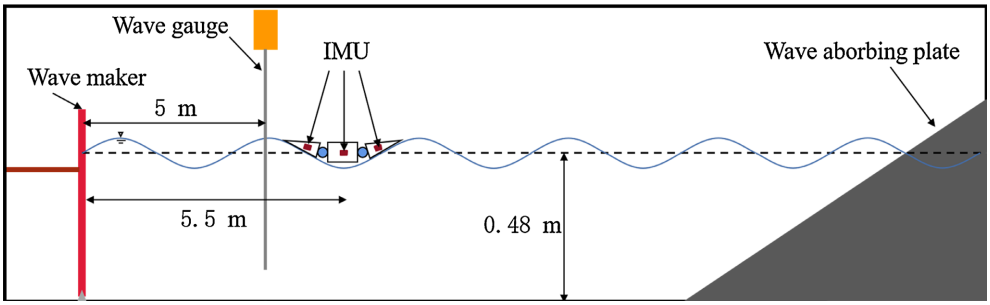

Figure 5. Experimental devices and tank settings of the test.

(a) (b)

Figure 6. The environment of wave tank experiment (a) Multi-plate wave maker; (b) Model and wave probe settings.

We equipped the vessel with three WitMoition WT9011DCL-BT50 IMU to record the vessel motions caused by waves. The IMU were fastened to the vessel using adhesive tape and the array configuration is illustrated in Figure 7. The sampling frequency of the sensors is 50 Hz, and the sensor of the central torso module is defined as IMU0, the sensor of the left pectoral fin module as IMU1, and the sensor of the right pectoral fin module as IMU2.

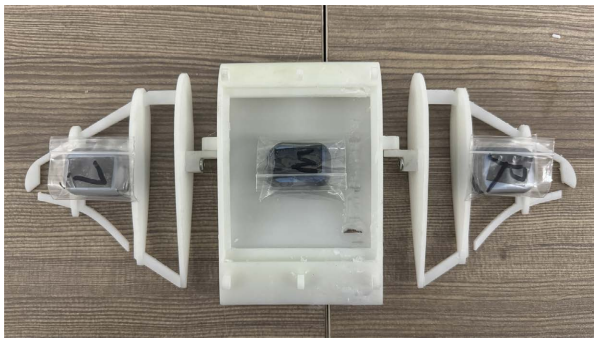

Figure 7. IMU settings on the manta bionic model.

3.2. Fixation of Model

Figure 8 illustrates the experimental setup with constrained position and heading. For each test configuration, identical elastic fixation bands are employed at all mooring points. Elastic ropes made of TPU are used as mooring lines, with a Young's modulus of 5.5×10^7 Pa. Each time the vehicle orientation is set, the initial elongation of each elastic rope is set to 1 cm. Each time the vehicle orientation is set, the initial elongation of each elastic cord is set to 1 cm. This means that for each test condition, the effect of the elastic cord on the vehicle's motion response should be the same.

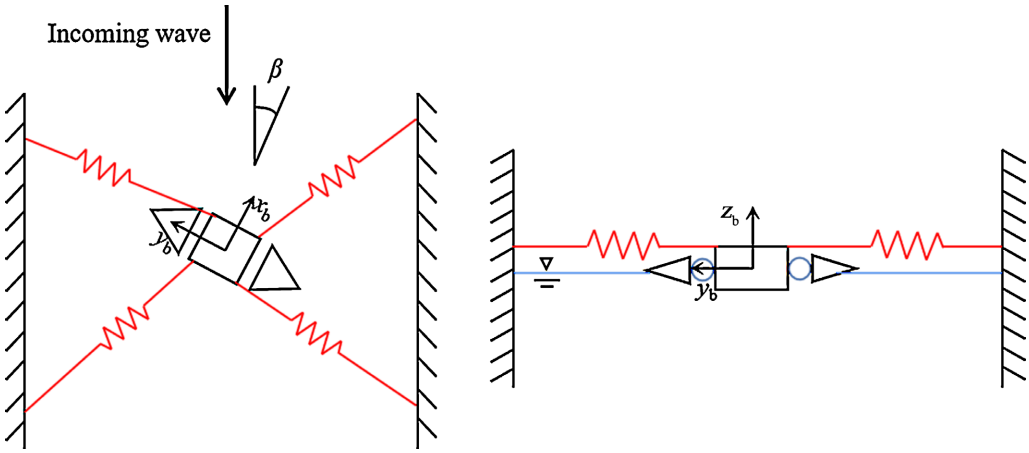

Figure 8. Illustration of fixation in experiment.

Horizontally oriented elastic bands maintain fixed model-wave alignment during testing. This arrangement:

1) Preserves constant relative orientation for directional response analysis

2) Strongly constrains horizontal-plane DOFs via tensile forces

3) Imposes negligible restrictions on vertical DOFs

3.3. Experimental Condition Setting

Systematic basin testing quantified incident wave direction effects on vessel roll/pitch responses. Seven relative wave directions (β = 0˚, 30˚, 60˚, 90˚, 120˚, 150˚, 180˚) and three characteristic periods (T = 0.6 s, 0.7 s, 0.8 s) defined the test matrix. Each of the 21 unique conditions underwent triplicate regular wave exposures, yielding 63 experiments to ensure statistical significance and repeatability validation.

To validate the adjudication methodology, two representative wave directions were selected: β_{set} = 45˚ (head oblique wave segment, 0˚ - 90˚) and β_{set} = 135˚ (tail oblique wave segment, 90˚ - 180˚). Vessel roll and pitch motion time-series data were acquired under these conditions. All tests employed a constant wave height of H = 0.03 m.

Refer to a full-scale manta-ray vehicle with a similar manta ray-inspired structure that has already completed actual sea trials [10]. Its wingspan is 3.2 m. Under the condition that the Froude number remains the same, when the scale ratio is 1:10, the corresponding actual wave amplitude is 0.3 m. According to the International Wave Scale, an actual sea wave height range of 0.1 - 0.5 m falls within the "smooth wave" category. Within this range, small vehicles such as manta-ray vehicles are suitable for operating on the sea surface.

4. Result and Discussion

4.1. Motion in Roll and Pitch

The motions under regular wave stimulation in roll, pitch are presented here. Results for incident regular waves with a wave period of 0.8 s and a wave height of 0.03 m is chosen to present in this segment as an illustration of the amplitude difference between roll and pitch motion.

Figures 9-11 show the vessel responds differently to roll and pitch motion in facing, backing, and transverse incoming waves. The central module of the vehicle exhibits a pitch motion with an average maximum amplitude of 6 degrees for regular waves in the 0˚ and 180˚ wave directions, whereas the roll motion exhibited by the downward module for both types of waves has an average maximum amplitude of only about 0.5 degrees, while the opposite is true for waves in the 90˚ wave direction.

Figures 12-15 show the roll and pitch motion response signals of the vehicle measured at wave directions of 30, 60, 120, and 150 degrees, respectively. Figure 16 presents the phase difference for all these 4 headings evaluated, where each color represents one heading. For 30˚ and 60˚ heading the phase difference is very similar, while 120˚ and 150˚ are in anti-phase.

4.2. Estimating Wave Direction of Incoming Wave from Difference in Roll and Pitch

Based on the roll, pitch and relative incident wave direction correlation of the

central module of the vessel shown in segment **2.3**, the power spectrum data of the roll and pitch motion response data of the central torso module are computed and processed based on the principle of orientation of the two-axis tachometer to obtain the power spectrum data of the roll and pitch motion response data of the central torso module, and the judgemental parameter curves are computed by the equation (3) as shown in Figure 17.

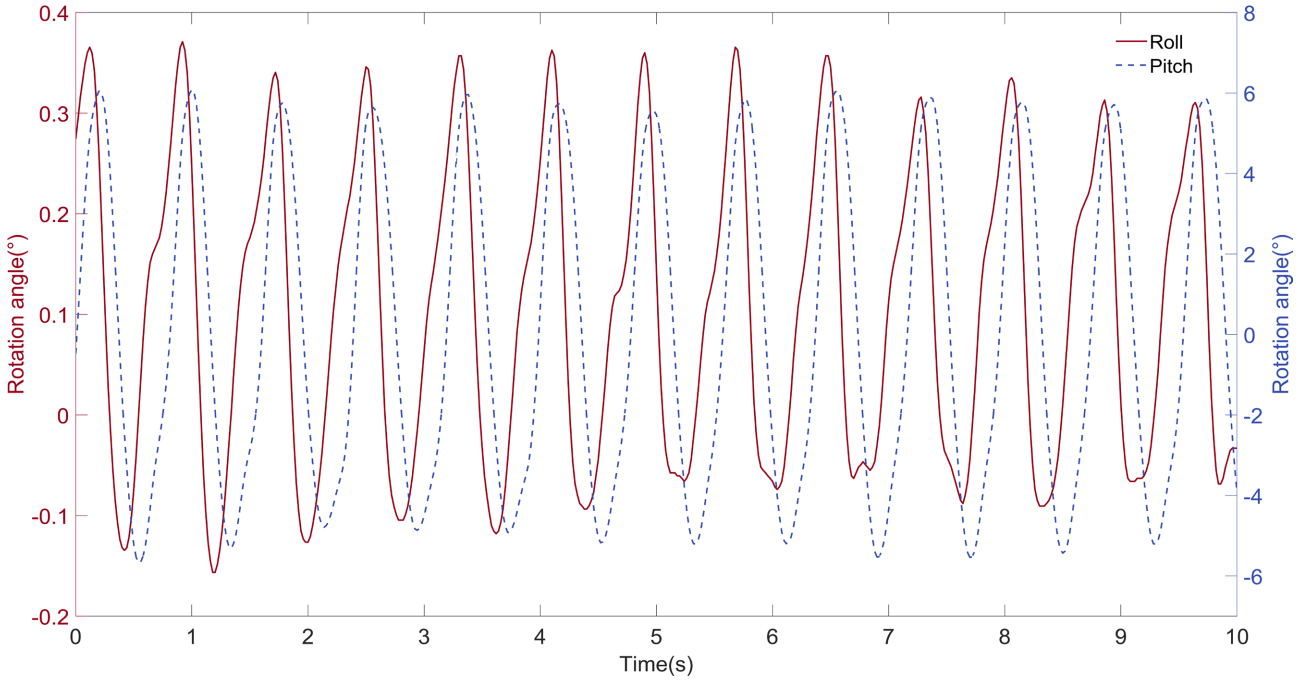

Figure 9. $T = 0.8$ s, $H = 0.03$ m, $\beta = 0^{\circ}$, roll and pitch time series data.

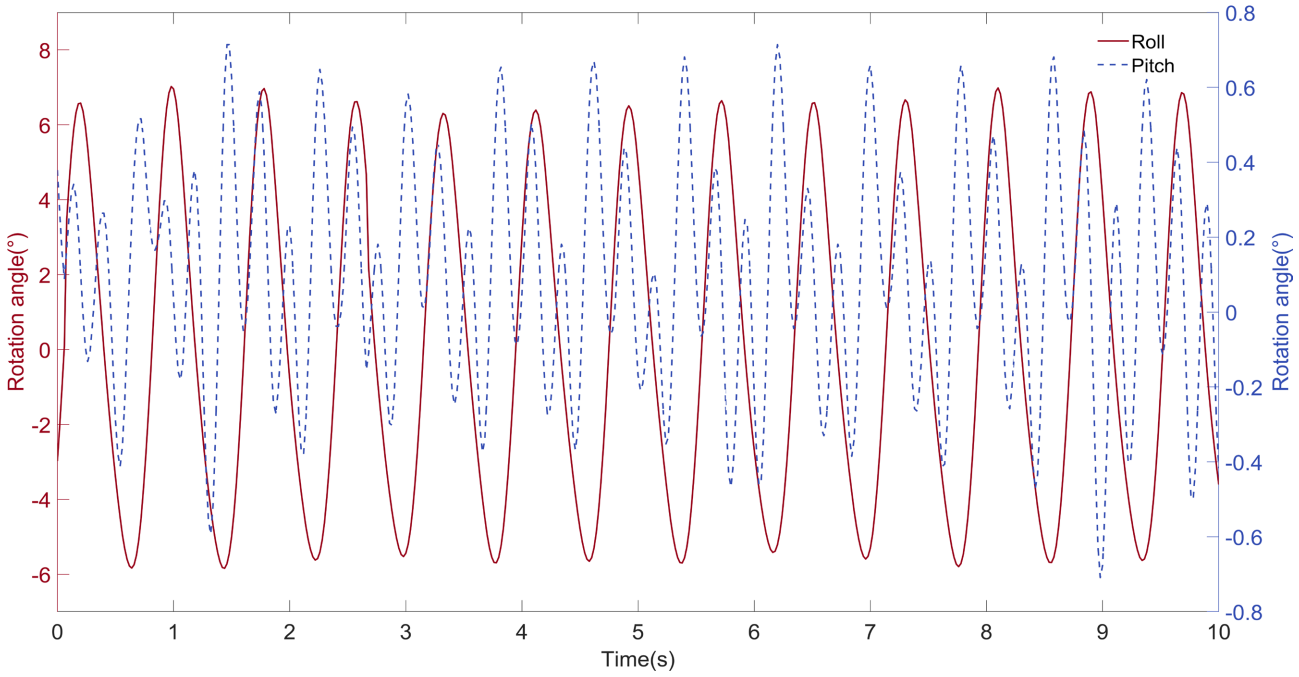

Figure 10. $T = 0.8$ s, $H = 0.03$ m, $\beta = 90^{\circ}$, roll and pitch time series data.

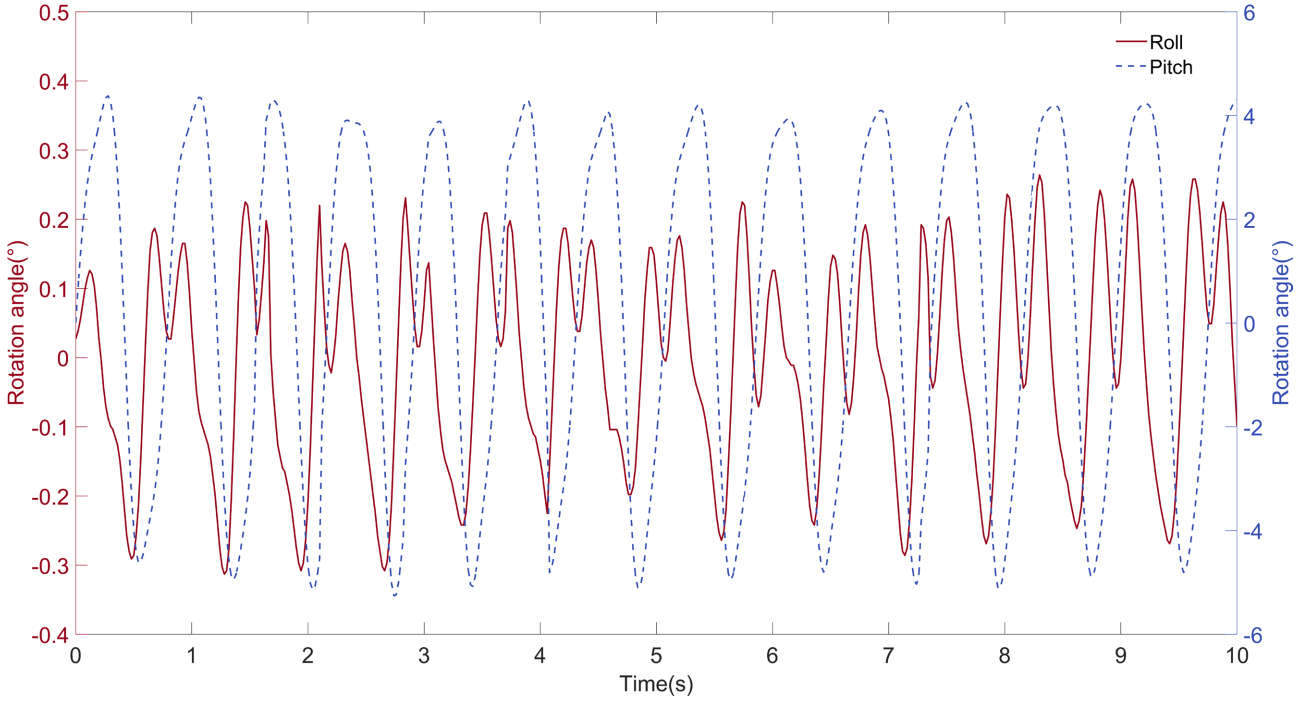

Figure 11. $T = 0.8$ s, $H = 0.03$ m, $\beta = 180^{\circ}$, roll and pitch time series data.

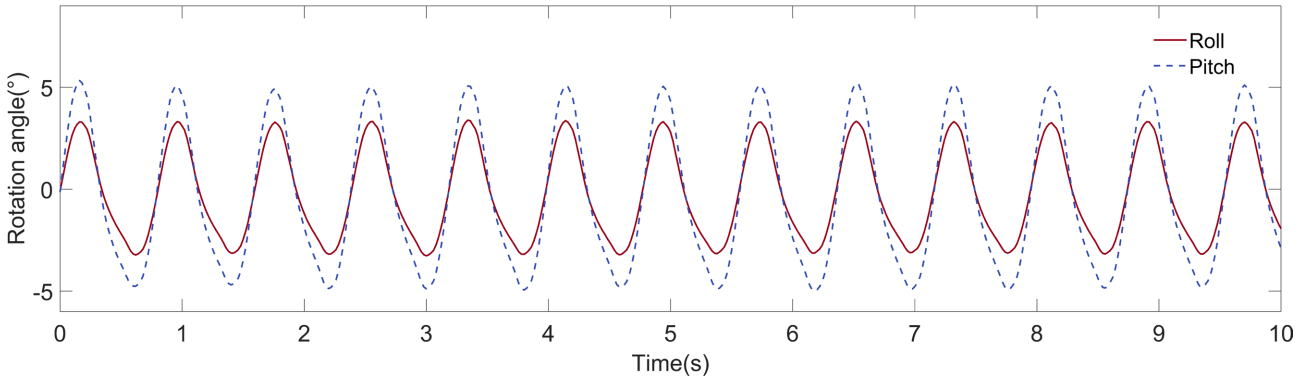

Figure 12. $T = 0.8$ s, $H = 0.03$ m, $\beta = 30^{\circ}$, roll and pitch time series data.

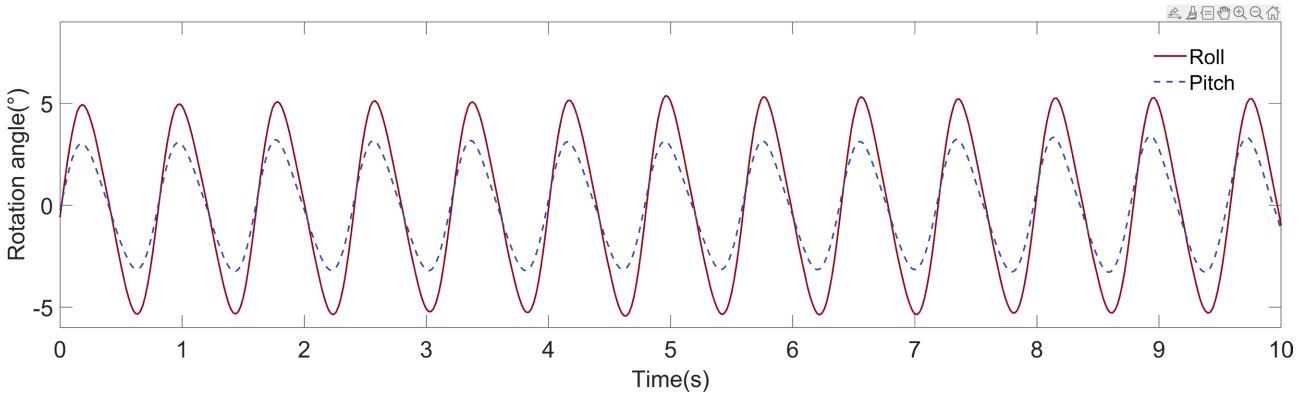

Figure 13. $T = 0.8$ s, $H = 0.03$ m, $\beta = 60^{\circ}$, roll and pitch time series data.

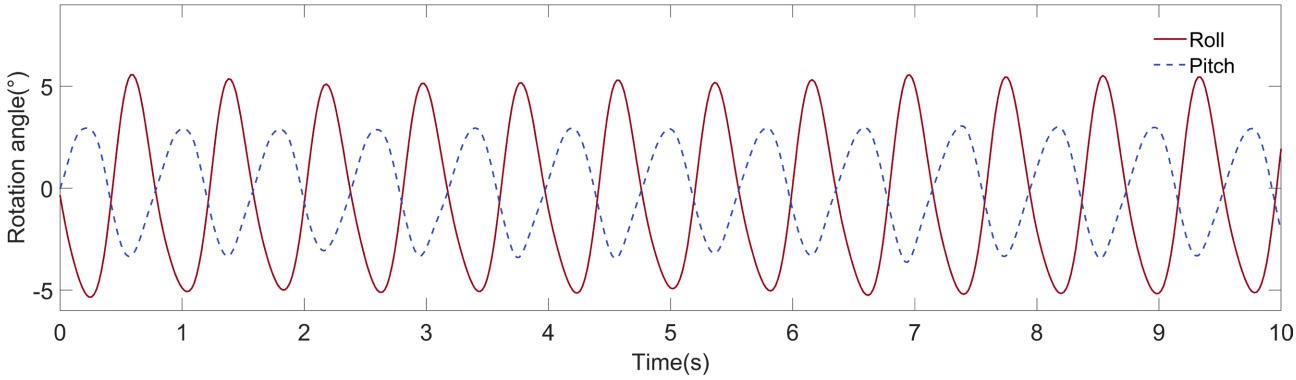

Figure 14. $T = 0.8$ s, $H = 0.03$ m, $\beta = 120^{\circ}$, roll and pitch time series data.

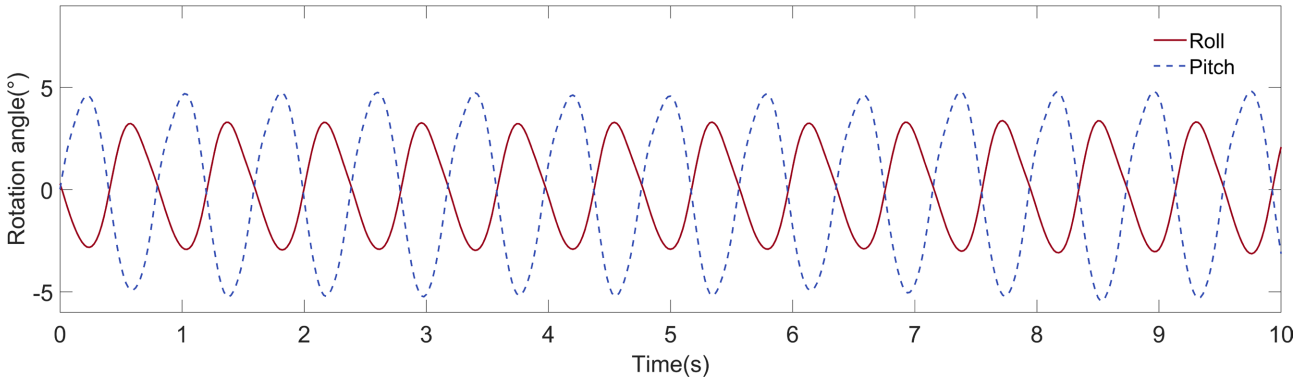

Figure 15. $T = 0.8$ s, $H = 0.03$ m, $\beta = 150^{\circ}$, roll and pitch time series data.

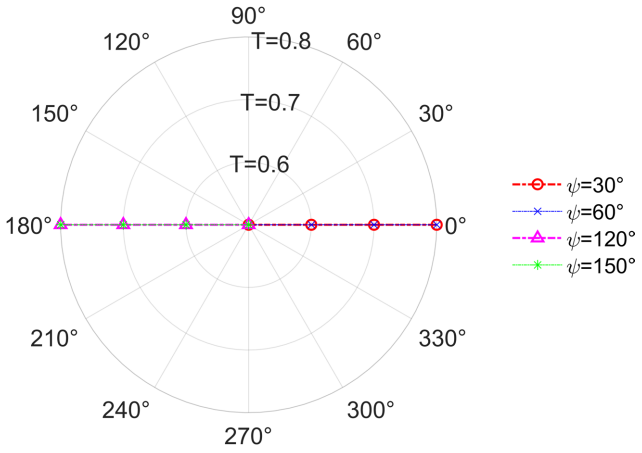

Figure 16. Phase difference in roll and pitch. Each radius corresponds to the specified wave period, and the polar radius represent the phase difference between roll and pitch. The different colors represent different headings of the model.

Figure 17 depicts the relationship between the judgment parameters *K1* and *K2* and the incident regular wave period and the relative incident wave direction. Under the condition that the wave period of the incident regular wave remains constant, the orientation parameter *K1* is symmetric to the transverse wave direction, and the range of the wave direction and the relative incident wave direction are nonlinear in the head oblique and tail oblique segments. The judgment parameter *K2* roughly reflects the energy ratio between the roll and pitch motion responses

of the central torso module of the manta ray bionic multi-modular vehicle model under the incident regular waves in different wave directions, and the wave direction segmentation is more pronounced than that of the parameter *K1* in the wave direction ranges of the head and tail oblique segments.

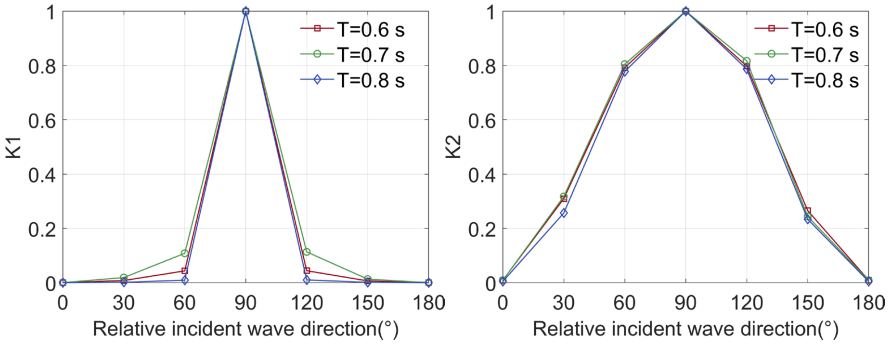

(a) (b)

Figure 17. Wave direction estimation parameters curves (a) *K*1; (b) *K*2.

The validity of the main wave direction estimation method in this paper is verified by collecting the roll and pitch time series data of the navigator under the action of the regular wave in two wave directions, 45˚ and 135˚. Three sets of roll and pitch motion response time series data of the manta ray bionic vehicle were obtained from the wave flume experiments for the central torso module of the vehicle at wave height H = 0.03 m, wave period (T = 0.6 s, 0.7 s, 0.8 s), and the relative incident wave direction (β_{set} = 45˚, 135˚) incident regular waves. The three sets of motion response data under the same period are sequentially numbered as #1~#3.

Based on the above sets of time series data of roll and pitch motion response of the vehicle, the phase difference is calculated to differentiate the relative incident wave directions of the first oblique and tail oblique segments. After selecting the wave direction segments, the corresponding roll and pitch motion power spectra were calculated by the periodogram method based on the motion response data. Then, the judgment parameter *K*2 is calculated from the power spectra of the roll and pitch motion time-series data, and the current main wave direction of the vehicle is estimated from the results of the judgment parameter curve, and the main wave direction estimation results are shown in **Figure 18**. The curves are the head and tail oblique sections of the *K*2 curve in **Figure 17(b)**, and the markers on the curves indicate the current wave direction calculated from the pitch and roll motion responses of experimental groups #1, #2 and #3, respectively.

The relative errors were calculated based on the main wave direction estimation results of each group, as shown in **Table 1**. The maximum relative error of the estimated results of this wave direction estimation experiment is 15.00%. It can be seen that the manta ray bionic multi-module navigator model has a good wave-following property, and is able to obtain the current main wave direction information of the navigation through the main wave direction estimation method based on

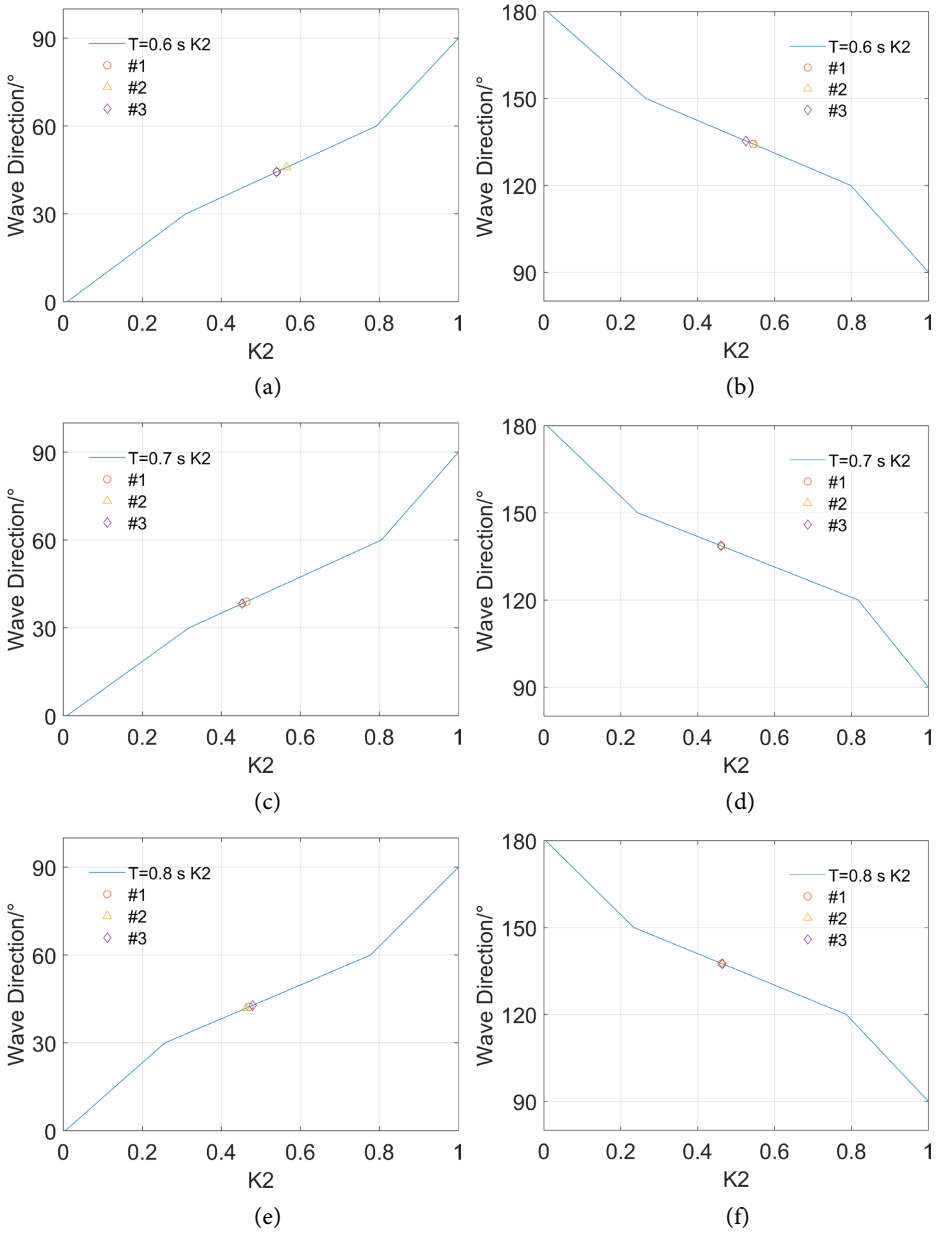

Figure 18. Wave direction estimation results of (a) T = 0.6 s head oblique segment; (b) T = 0.6 s tail oblique segment; (c) T = 0.7 s head oblique segment; (d) T = 0.7 s tail oblique segment; (e) T = 0.8 s head oblique segment; (f) T = 0.8 s tail oblique segment.

Table 1. Comparison of wave direction settings and estimates.

T(s)	Relative error in wave direction estimation					
	β_{set} = 45˚			β_{set} = 135˚		
	#1	#2	#3	#1	#2	#3
0.6	1.45%	1.98%	1.52%	0.51%	0.78%	0.27%
0.7	13.34%	15.00%	14.87%	2.70%	2.61%	2.71%
0.8	5.87%	7.03%	8.00%	1.93%	1.92%	1.85%

the principle of orientation of the two-axis tachometer, using the roll and pitch rocking motion response data of the central torso module of the navigator.

5. Conclusion and Further Work

5.1. Conclusions

Under regular wave incidence, the judging parameter curve $K2$, computed from the roll and pitch motion signals of the central torso module of the manta ray bionic multi-modular vehicle, is approximately symmetric about the transverse wave direction. This curve exhibits a phase difference in the motion response signal in the head oblique wave direction segment, while showing a phase difference of size π in the tail oblique wave direction segment. Based on the correlation between the roll and pitch motions of the vehicle model and the incident wave direction, the ratio of the principal energies of the two motions can be utilized for the estimation of the principal wave direction.

The judgment parameters $K1$ and $K2$ reflect the inherent relationship between the roll and pitch motion response of the central torso module of the navigator, the incident wave period, and the relative incident wave direction. They possess characteristics that are clearly related to the relative incident wave direction, reflecting the inherent motion characteristics of the navigator in regular waves. Once the shape and structure parameters of the vehicle are determined, numerical simulation and wave tank experiments can be conducted to calculate the wave direction estimation parameters in advance. This enables the determination of the current main wave direction of the vehicle according.

Current mainstream methods for estimating wave direction spectra, such as the direct Fourier transform, Fourier series expansion, and maximum likelihood estimation approaches, generally require 3 - 6 input signals and often encounter computational convergence stability challenges. In contrast, the primary wave direction estimation method employed in this study demonstrates significant advantages by requiring only two motion signals (roll and pitch) to accurately determine the vehicle's prevailing wave direction. This innovative approach achieves satisfactory estimation accuracy while substantially reducing both the number of required measurement signals and computational complexity.

5.2. Further Work

Several promising avenues warrant further investigation. A key limitation of the current experimental setup is that the restraining straps restrict the vessel's motion in multiple degrees of freedom (DOFs). Analyzing the roll and pitch responses of a freely floating vehicle across different wave headings would provide valuable insights into the applicability of this primary wave direction estimation method in real-world maritime conditions. Such an investigation represents a compelling direction for future research.

This study measured and recorded roll and pitch motion response signals of the manta ray vehicle under various regular wave conditions. The primary wave di-

rection was estimated by analyzing the correlation between these motion signals and the relative wave incidence direction. However, actual sea states present more complex wave environments where the vehicle encounters multi-directional wave interference. Future research will investigate the vehicle's performance under irregular wave conditions to better simulate real-world ocean environments.

Acknowledgements

This work is supported by Shenzhen Science and Technology Program of China (No. JCYJ20220818102012024).

Conflicts of Interest

The authors declare no conflicts of interest regarding the publication of this paper.

References

[1] Chen, W., Lu, Y., Li, S. and Gao, F. (2023) A Bio-Inspired Foldable-Wing Wave Energy Converter for Ocean Robots. *Applied Energy*, **334**, Article 120696. https://doi.org/10.1016/j.apenergy.2023.120696

[2] Chen, W., Lin, X., Lu, Y., Li, S., Wang, L., Zhang, Y., *et al.* (2023) Design and Experiment of a Double-Wing Wave Energy Converter. *Renewable Energy*, **202**, 1497-1506. https://doi.org/10.1016/j.renene.2022.12.033

[3] Wang, J.M., Yang, P. and Li, J.R. (2023) Hydrodynamic Analysis and Energy Capture Efficiency of Multi-Module Bionic Manta Ray UUV. *Chinese Journal of Ship Research*, **18**, 106-118.

[4] Qin, Y.C., Huang, L.M., Ma, X.W. and Duan, W.Y. (2021) Summary of Research Progress on Ship Analog Wave Buoy Technology. *Proceedings of the* 16*th National Conference on Hydrodynamics and the* 32*nd National Symposium on Hydrodynamics*, **2**, 645-652.

[5] Dirdal, J.A., Skjetne, R., Roháč, J. and Fossen, T.I. (2022) Online Wave Direction and Wave Number Estimation from Surface Vessel Motions Using Distributed Inertial Measurement Arrays and Phase-Time-Path-Differences. *Ocean Engineering*, **249**, Article 110760. https://doi.org/10.1016/j.oceaneng.2022.110760

[6] Dirdal, J.A., Skjetne, R., Roháč, J. and Fossen, T.I. (2023) A Phase-Time-Path-Difference Approach for Online Wave Direction and Wave Number Estimation from Measured Ship Motions in Zero and Forward Speed Using a Single Inertial Measurement Unit. *Ocean Engineering*, **288**, Article 116131. https://doi.org/10.1016/j.oceaneng.2023.116131

[7] Selimović, D., Hržić, F., Prpić-Oršić, J. and Lerga, J. (2023) Estimation of Sea State Parameters from Ship Motion Responses Using Attention-Based Neural Networks. *Ocean Engineering*, **281**, Article 114915. https://doi.org/10.1016/j.oceaneng.2023.114915

[8] Cai, W., Zhan, J. and Luo, Y. (2020) A Study on the Hydrodynamic Performance of Manta Ray Biomimetic Glider under Unconstrained Six-DOF Motion. *PLOS ONE*, **15**, e0241677. https://doi.org/10.1371/journal.pone.0241677

[9] Jiang, L. (2004) Forecasting Sea Waves Based on the Motion of Ships in Navigation. Ph.D. Thesis, Harbin Engineering University.

[10] Zhang, D., Pan, G., Cao, Y., Huang, Q. and Cao, Y. (2022) A Novel Integrated Gliding and Flapping Propulsion Biomimetic Manta-Ray Robot. *Journal of Marine Science and Engineering*, **10**, Article 924. https://doi.org/10.3390/jmse10070924